Green Synthesis of Few-Layer Graphene for Supercapacitor Applications via Mechanical Exfoliation using A High-Speed Kitchen Blender

Pakhawat Insuwan[1], Montri Luengchavanon[2,*], and Natthaporn Kaewchoothoong[3],

[1]Faculty of Environmental Management, Prince of Songkla University, Songkhla 90110, Thailand

[2]Sustainable Energy Management Programme, Wind Energy and Energy Storage Systems Centre (WEESYC), Faculty of Environmental Management, Prince of Songkla University, Songkhla 90110, Thailand

[3]Department of Mechanical and Mechatronics Engineering, Faculty of Engineering, Prince of Songkla University, Songkhla 90110, Thailand

(*Corresponding author's e-mail: montri.su@psu.ac.th)

Abstract

Supercapacitors (SCs) have the potential to be reliable energy storage devices. They offer high-power, a long life cycle, and excellent reliability, making them ideal for consumer electronics. Numerous studies have focused on developing carbon-based materials with a high specific surface area and electronic and ionic conductivity that leads to the provision of high specific capacitance. Few-layer graphene (FLG) has garnered significant attention due to its exceptional electrical, mechanical, and thermal properties. This study introduces a simple, scalable, and eco-friendly approach to synthesizing FLG through mechanical exfoliation using a high-speed kitchen blender. The process employs graphite and Pluronic F-127 surfactant in an aqueous solution, ensuring reduced environmental impact. Structural analysis via Raman and FTIR spectroscopies and XRD confirmed successful exfoliation with minimal defects, and retention of the graphitic framework. TEM images demonstrate approximately 400 nm diameter, uniformly shaped, well-ordered nanosheets. Electrochemical characterization highlights the suitability of FLG electrodes for supercapacitors, while cyclic voltammetry (CV) displays excellent reversibility, and EIS demonstrates a low charge transfer resistance ($\sim$0.15 Ω). The fabricated FLG-based supercapacitor achieved specific capacitances up to 71.34 F g^{-1} under a low current density, confirming high energy storage efficiency. The combination of simplicity, scalability, and cost-effectiveness makes this method promising for large-scale production, fostering advances in sustainable energy storage technologies.

Keywords: Green synthesis, Single step, Mechanical exfoliation, Supercapacitor, Few-layer graphene, Shear exfoliation, Pluronic F-127 surfactant

Introduction

Nowadays, supercapacitors have become a fascinating form of energy storage: Especially the electrical double layer super capacitors (EDLCs) offer a number of benefits, including high power (>10 kW kg^{-1}), long cycle lives (over 10^5 cycles), and excellent reliability, making them ideal for consumer electronics, rapid start-stops, and high-speed transportation systems [1]. Presently, graphene oxide (GO) has garnered substantial attention due to its exceptional electrical and chemical properties. These properties include remarkably high electrical conductivity ($\sim$$10^6$ S cm^{-1}),

significant specific surface area ($\sim$2,630 m^2 g^{-1}), excellent thermal conductivity ($\sim$5,000 W mK^{-1}), and high chemical stability [2,3]. Many processes have been developed to generate GO in large-scale production for applications. Those processes include mechanical [4], chemical [5], electrochemical [6], and thermal exfoliation [7], and they commonly break down graphite to intercalated layers, used to achieve percolation and network formation inside a polymer matrix [8]. Paton *et al.* [9] showed a method of shear-exfoliating graphite to produce GO industrially scalably. This entails

producing GO in stabilizing solvents as well as polymer or surfactant solutions, utilizing a high-shear rotor-stator mixer. However, there are certain drawbacks to this strategy. This approach yields only modest concentrations ($C \approx 0.1$ mg mL^{-1}), restricting the rate of production. Still, the inherent benefits of shear exfoliation more than compensate for the obstacles. The problems described above are most likely connected to the specifics of the rotor-stator generating the shear flow. Other approaches to generate high shear in a scalable manner without the difficulties stated above may exist [9]. A completely developed turbulence along with the high-shear zones is required to address the limitations of the rotor-stator mixer. Alhassan *et al.* [10] first established the viability of exfoliating graphite through turbulent mixing using a stainless steel blender with a 4-blade impeller. However, they skipped over the further optimization to obtain mostly monolayer GO; instead, they only concentrated on this initial notion employing laponite. Recently, this method has been promoted by Yi *et al.* [11]; Varrla *et al.* [12]. Measurements in many groups have demonstrated that graphite can be exfoliated to produce GO using a simple, high-speed rotating blade.

Table 1 Comparison of methods for GO production [14].

Property	Mechanical exfoliation	Chemical exfoliation	Chemical vapor deposition
Production method complexity	Low	Medium	Very High
Quality of synthesized GO	Very High	Poor	High
Production price (per 1 cm^2)	-	<0.1 USD	<1 USD
Feasibility of single-layer GO production	Yes, but with difficulties	No	Yes
Scalability	Scalable [13]	Scalable	Scalable

shows a comparison of GO production methods by mechanical or chemical exfoliation, and by chemical vapor deposition. The mechanical exfoliation demonstration was based on a kitchen blender, and is scalable by modification to the control loop and speed, while able to achieve 2% mass yield on average for 5-layer GO after 30 min (Kenwood blender with a water/NaC dispersant, [13]). The low cost of mechanical exfoliation may be inferred from the low complexity of the production method. Mass production of graphene nano-sheets mainly uses mechanical or electrochemical exfoliation [15].

In addition, the choice of surfactant greatly influences the efficiency of exfoliation and dispersion stability, as well as the overall quality of the GO layers obtained. Surfactants can reduce the surface tension and interfacial energy of GO, thus easing the separation of graphite layers [16], preventing re-aggregation of exfoliated GO by electrostatic or steric stabilization, maintaining uniform dispersion [17], and improving the yield and quality of exfoliated GO by maintaining structural integrity and minimizing structural defects [18]. Karagiannidis *et al.* [19] exfoliated graphite into GO through microfluidics using sodium deoxycholate as surfactant, to provide smaller pristine graphitic particles from 8 to 1 μm. Moreover, highly concentrated GO dispersions from exfoliating graphite using the solvent N-methyl-2-pyrrolidone was demonstrated by Khan *et al.* [20] achieving stable dispersions of up to approximately 63 mg mL^{-1} [20].

In this current study, a novel and simplified approach was demonstrated for the preparation of few-layer graphene (FLG) through mechanical high-speed blending (23 krpm) in the presence of Pluronic F-127, tuned by varying the solvent concentration (C_s), initial graphite concentration (C_i), and mixing time (t). Contrary to traditional techniques such as Hummers' oxidation or probe sonication, this comparatively low-energy method produces FLG with moderate quality and electrochemical activity that allow fabricating electrodes for supercapacitor applications with 6 M KOH electrolyte.

Materials and methods

Graphite powder (size 10 μm) was purchased from Tiger Rich System Co., Ltd., and used as supplied. The surfactant used was Pluronic F-127 (PF-127), which was purchased from Sigma Aldrich. In this research, a Sharp blender (model emc-15) was used to disperse and exfoliate graphite powder in PF-127 solution. To execute each mix, the required quantity of PF-127 was dissolved in 200 mL of deionized water by stirring. The tapered blender jug was given the dose of graphite, which was then topped with the PF-127-water solution. The kitchen blender (Sharp, EMC-15) of 2-liter capacity has a set of 6 blades (stainless material), with 4 blades (70 mm diameter) in the lower position and 2 blades (30 mm diameter) in the upper position. The blades are L-shaped in this commercially available kitchen blender. The blender was operated at full speed (23 krpm) for 10 - 60 min. Due to overheating, such blenders are not intended to be operated at high speeds for long periods of time. To deal with this, the blender was turned off for 1 min after each minute of mixing (1 min on/1 min off duty cycle). During the off cycles, the jug was immersed in a cold-water bath. After mixing, aliquots of the dispersions were collected and centrifuged (Dynamica, Velocity 18R with fixed angle rotor) at 1,000 rpm for 45 min.

The concentrations of FLG were determined using UV-Vis spectroscopy (PhotoLab 7600). To characterize the sample, Raman spectroscopy was used to determine the degree of graphitization in the GO materials as well as the I_{2D}/I_G intensity ratio [21]. In addition, the structure of GO was analyzed using X-ray diffraction (XRD, PANalytical Empyrean), and transmission electron microscopy (TEM, JOEL, JEM-2010) images were used to investigate the morphological properties of graphite nanostructures.

In testing the performance characteristics in a supercapacitor application, the current collectors were copper plates, and 2 sizes of FLG electrodes were prepared, with 1 cm^2 to conduct electrochemical impedance spectroscopy (EIS), and 1 g for cyclic voltammetry (CV) and galvanostatic charge/discharge (GCD). These characterizations were measured using Autolab PGSTAT302N. CV was recorded at various scan rates from 100 to 500 mV s^{-1} with a voltage range from −1 to 1 V, which aligns with the standard electrochemical stability window for aqueous electrolytes such as KOH [22]. This potential range is commonly used in supercapacitor studies to avoid water electrolysis while maximizing the accessible voltage window for double-layer formation. According to Kötz *et al.* [23], aqueous-based supercapacitors typically operate within this range to ensure stability and avoid parasitic faradaic reactions. EIS was recorded in the frequency range of 0.1 - 100,000 Hz by applying an AC voltage with 5 mV perturbation. The influences of FLG on electrochemical performance for supercapacitors were clearly revealed, and the results are expected to provide the experimental basis for further study on GO-based energy storage devices. Preparation of the supercapacitor cell made use of a 7×15 cm^2 cell sandwiched between acrylic materials (10 mm), stacked in the order acrylic/current collector coated with GO/separator paper saturated with 6 M KOH/current collector coated with GO/acrylic. Screws were used to press the layers together, and silicon glue was used for sealing. The 12 μm copper current collector was made in China (TMAXCN). A summary of the steps for this testing is as follows: (1) Prepare the graphite and aqueous suspension of Pluronic F-127 (PF-127). (2) Set up the kitchen blender (Sharp, EMC-15) and run shear flow following the experimental design. (3) Fine graphite suspension is collected and centrifuged (Dynamica, Velocity 18R with fixed angle rotor) to separate the generated GO. (4) The GO properties are measured, using TEM, UV-VIS, and XRD. (5) Prepare the supercapacitor with 1 g GO in the sandwich cell. (6) The electrochemical supercapacitor is tested for CV and GDC.

Results and discussion

The primary benefit of utilizing a rotating-blade mixer to generate FLG is its ability to treat relatively large liquid volumes quickly. Sonication probes, on the other hand, may efficiently treat quantities as little as a few hundred mL, resulting in modest output rates [20,24]. From this experiment, the supernatant concentration was determined using UV-Vis spectroscopy. The Lambert-Beer extinction law states that the optical absorbance is directly proportional to concentration using:

$$Ext = \varepsilon C_G l \qquad\qquad (1)$$

where Ext is the extinction, ε is the extinction coefficient, C_G is the concentration, and l is the path length [25]. The extinction of an extracted sample from each system was measured at 660 nm in a cell with a 10-mm path length. FLG dispersions in surfactant/water solutions were found to have an extinction coefficient of 1,330.5 mL mg^{-1} m^{-1}.

PF-127 was set at 1 g or 2 g (PF1 and PF2) in 200 mL DI water, with shearing in blender for 10 min, to test the effects of Pluronic surfactant concentration.

Error! Reference source not found.**(A)** indicates that as the concentration of graphite increased, the concentration of FLG also grew. The highest FLG concentration was achieved using PF1 and PF2 at 20 g of graphite and 10 min of exfoliation time, yielding 1.52 and 2.49 mg mL^{-1}, respectively. This suggests that the PF2 process might have enhanced efficiency in producing FLG, potentially due to surfactant interactions. In addition, the yield of FLG as a percentage (Error! Reference source not found.**(B)**) decreased with the concentration of graphite. PF1 generally shows higher yield (17.94%) compared to PF2 (14.28%) at the lower graphite concentrations, but decreases sharply as graphite increases. Additionally, the production rate of FLG (**Error! Reference source not found.**C) had an increasing trend with the concentration of graphite. This indicates that, despite the drop in yield, the total amount of FLG produced per unit of time does rise with amount of graphite input.

Moreover, as blending time increases in Error! Reference source not found.**(D)**, where PF1Ci1 has PF-127 1 g and graphite 1 g, PF2Ci20 has PF-127 2 g and graphite 20 g, the concentration of FLG grows for both conditions, though PF2Ci20 exhibits a steeper rise, reaching its peak at 60 min with a maximum concentration of 6.39 mg mL^{-1} and standard deviation of 0.187, **Figure 2** Concentration of mechanically

exfoliated GO as a function of exfoliating time in data curated from the literature (**Table 2** for details). The current study is number 12 in this plot.

Table 1 [26]. PF1Ci1 shows a slower but steady increase to 2.09 mg mL^{-1} at 60 min, implying a gradual improvement in dispersion over time. In Error! Reference source not found.**(E)**, the yield of FLG improves over time in PF1Ci1 but remains low and steady in PF2Ci20, particularly after the 30-minute mark. In PF1Ci1, the extended blending time contributes positively to the exfoliation efficiency, which reaches a peak 41.85% yield. In contrast, PF2Ci20 does not demonstrate significant yield improvements over time, suggesting that a higher initial concentration of graphite may limit the effectiveness of prolonged blending due to aggregation or stabilization challenges [12].

In Error! Reference source not found.**(F)**, the production rate starts higher in PF2Ci20 (0.23 mg mL^{-1} min^{-1}) at the 10-minute mark, suggesting an initially efficient process, but it stabilizes as time progresses. This could indicate rapid initial exfoliation followed by saturation or agglomeration effects. The technique used in this work is more effective at producing high concentrations of 6.39 mg mL^{-1} GO dispersions when compared to comparable mechanical exfoliation techniques for GO that have been documented in the literature, as illustrated in **Figure 2** and **Table 2**. This study demonstrates high efficiency in FLG production within a short exfoliation time while achieving the highest GO concentration. The results highlight the effectiveness of the process in maximizing yield with minimal processing duration [27-34].
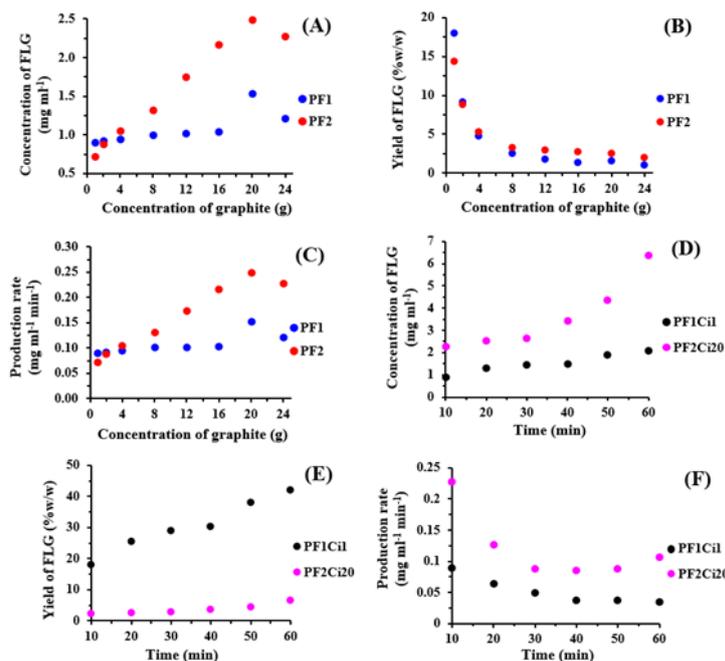
Figure 1 A comparison between amounts of PF-127 set at 1 g or 2 g (PF1 and PF2) in DI water, sheared for 10 min. (A) Concentration of mixer-dispersed FLG plotted against graphite concentration C_i, (B) yield of FLG, which was calculated from C_{FLG}/C_i plotted against C_i, (C) production rate, which was calculated from C_{FLG}/time plotted against C_i, (D) plot of C_{FLG} against time, (E) plot of yield of FLG against time, and (F) plot of production rate against time. (D) - (F) Comparison between PF1Ci1 and PF2Ci20.
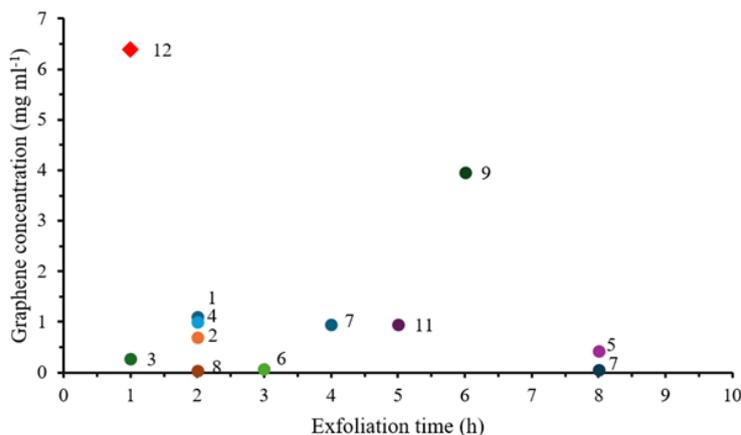

Figure 2 Concentration of mechanically exfoliated GO as a function of exfoliating time in data curated from the literature (**Table 2** for details). The current study is number 12 in this plot.

Table 1 Experimental repetitions and measurement uncertainties.

Number	Methodologies	Concentration (mg mL^{-1})	Average (mg mL^{-1})	Standard deviation (Error)
1		6.18		
2	Rotating blade blender	6.45	6.39	± 0.187
3		6.54		

The number of experimental repetitions along with the measurement uncertainty for 3 repetitions: 6.39 mg mL^{-1} with ± 0.187 standard deviation (error).

Table 2 The concentration of GO produced mechanically by exfoliation for a given time, in data curated from the literature.

No. on graph	Method	Exfoliation medium	Time (h)	Concentration (mg mL^{-1})	References
1	Shear exfoliation	Water-sodium cholate solution	2	1.1	[27]
2	Shear exfoliation	Polyvinylpyrrolidone	2	0.70	[27]
3	High shear mixer	IPA-water	1	0.27	[28]
4	Ultrasonic bath	water	2	1.00	[29]
5	Sonication (sequential)	NMP	8	0.43	[30]
6	Tip sonication	NMP/azobenzene	3	0.07	[31]
7	Bath sonication	Water/ammonia solution	8	0.058	[31]
8	Sonic bath	Aqueous ammonia	2	0.03	[32]
9	Shear exfoliation	Water/graphite oxide	6	3.96	[33]
10	Sonication bath	Urea	4	0.95	[34]
11	Sonication bath	NMP	5	0.95	[34]
12	Rotating blade blender	Pluronic f-127	1	6.39	This work

The household blender created a fully turbulent flow to produce GO. The shear rate reduces as the distance from the blade increases, while turbulence is well-developed throughout the fluid. As shown in Error! Reference source not found., the exfoliation mechanisms can involve high shear and collisions primarily caused by turbulence. Five fluid dynamics events are believed to cause the exfoliation and fragmentation, based on the properties of the turbulent flow in the kitchen blender [11], as follows:

(I) The steric repulsion force at the hydrophobic tails (hydrocarbon chain) of the surfactant molecules [35]. The interaction force and corresponding energy between 2 polymer-coated sheets were modeled by De Gennes [36], and the force per unit area is provided by the formula

$$F = \frac{k_b T}{D^3}\left[\left(\frac{h_c}{h}\right)^{9/4} - \left(\frac{h_c}{h}\right)^{3/4}\right] \qquad (2)$$

in which h_c denotes the chain length of the attached molecule that is stuck on the sheet, and D is the average distance between the 2 junction sites that link the sheet and the adhered molecule. The first term in the brackets indicates osmotic force, whereas the second represents elastic force. At high compressions, the osmotic term should dominate fully. In this model the interaction force is inversely proportional to the third power of D [37].

(II) Intensive Reynolds shear stress (Re$_{Blade}$) above the critical value $\sim 10^4$ can be caused by turbulence [12].

$$Re_{Blade} = ND^2\rho/\eta \qquad (3)$$

where ρ and η represent the liquid density (1,000 kg m^{-3}) and viscosity (0.001 Pa s), respectively. When N reaches its maximum value in the blender used (23 krpm), Re$_{Blade}$ > 10^6 is significantly higher than 10^4, indicating fully established turbulence.

(III) Due to the high Reynolds number and associated turbulence which favors inertial forces over viscous forces, graphite-graphite and edge collisions are enhanced [28].

(IV) It is probable that a pressure difference caused by turbulent pressure fluctuations also exfoliates graphite using normal forces [38].

(V) The viscous shear stress in confined laminar regions is proportional to the velocity gradient [39]:

$$\tau = \eta \frac{du}{dy} \qquad (4)$$

where τ represents the shear stress (Pa), η serves as the dynamic viscosity of the fluid (Pa s) and $\frac{du}{dy}$ means the velocity gradient (s^{-1}).

The key factors in GO production were Pluronic F-127 and high-speed rotation. Triblock copolymer Pluronic F127 has been demonstrated to disperse GO in electrolyte solution and block the hydrophobic interaction between GO and l-tryptophan and l-tyrosine, while pressure from the blades of the blender can be used to fabricate high concentration GO [40]. Therefore,

while the household blender produced simply GO, adding Pluronic F127 in the process enabled low-cost and 1-step production. The other methodologies reported are very complicated and have a high cost. Based on the turbulent flow in a blender with high-shear regions, 1-step mechanical exfoliation was enabled by Pluronic F127 surfactant that helped disperse and preserve the generated GO. This investigation has demonstrated a "green synthesis" because of the simple method, the low cost, and the low waste from the process.
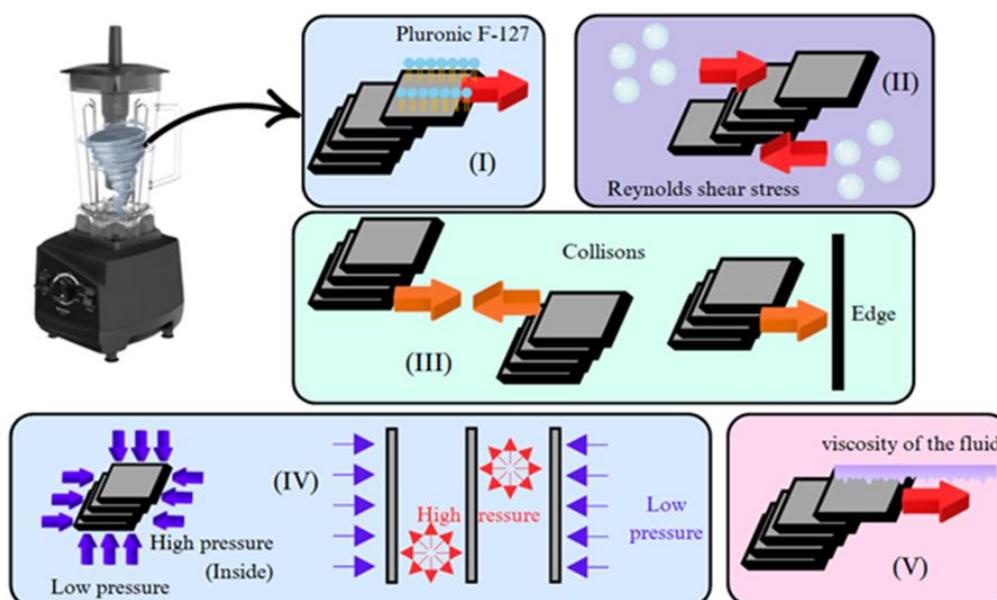

Figure 3 An illustration of the blender with a schematic of the mechanisms of exfoliation.

The TEM images in **Figure 4** depict the morphology and crystalline structure of the FLG synthesized. The layered arrangement of GO sheets with diameter 400 nm and clear interlayer spacing, confirms the high structural quality of the FLG. The visible straight and parallel edges suggest well-ordered layers with minimal structural defects, critical for maintaining the unique electrical and mechanical properties of GO [41]. The distinct interplanar distances indicate the presence of turbostratic or few-layer stacking rather than bulk graphite [42]. The sharp edges and consistent thickness across the layers point to a precise exfoliation process, likely minimizing layer damage and defects.

The high degree of crystallinity suggests that the synthesis technique effectively preserves the intrinsic properties of GO.

In this study, size selection of FLG was achieved through controlled centrifugation at 1,000 rpm for 45 min. This step separates smaller flakes from residual graphite. According to the method exhibited by Khan *et al.* [43], such a centrifugation rate typically results in flakes with a lateral dimension of ~1.6 μm. This indicates that the exfoliation and size selection in this study is consistent with best practices for producing FLG with improved structural quality and uniformity.
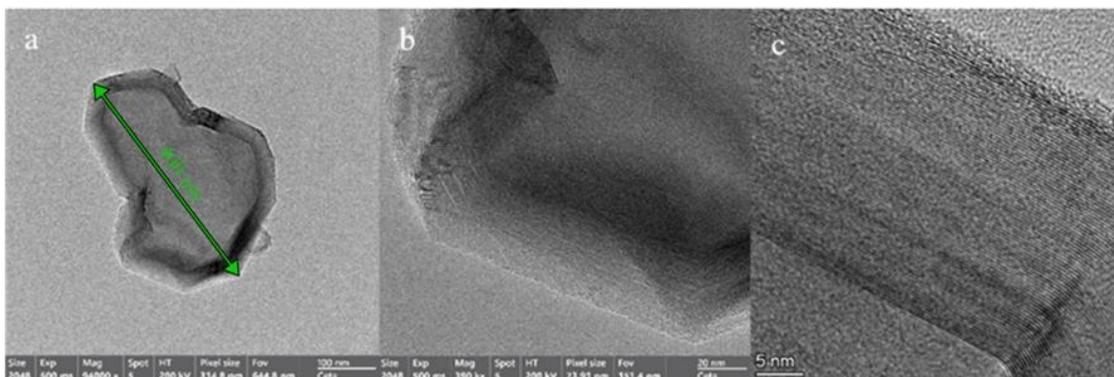
Figure 4 (a) TEM image of FLG, and high-resolution TEM images of FLG (b-c) revealing well-defined lattice fringes and layer stacking with nanoscale precision.

Raman spectra for graphite powder and FLG are shown in Error! Reference source not found.. Six peaks were identified in the Raman spectra. However, the significant peaks that identify carbon were at 1,341, 1,571, and 2,708 cm^{-1} due to D, G(E2g) and G'(2D) bands, respectively [44]. In other peaks, the Raman bands observed in graphite and FLG are caused by optical phonon scattering, which is an in-phase (coherent) oscillation of atoms from their equilibrium position [45,46]. Raman spectroscopy can also be used to demonstrate exfoliation, and it is one of the best non-destructive techniques for characterizing materials based on carbon. Both the thickness of GO sheets [47] and the quality of deposited GO layers [26] can be assessed using Raman spectroscopy.

The D-band ($\sim$1,350 cm^{-1}) is related to defects and disorder in the GO structure [48]. The D-band could be observed in the graphite spectrum, suggesting that there are some flaws. The D-band for FLG appears to be less strong or completely non-existent, indicating a lower defect density or higher structural quality than in graphite. In addition, the G-band ($\sim$1,580 cm^{-1}) refers to the in-plane vibrations of sp^2-bonded carbon atoms,

where carbon atoms in the hexagonal lattice vibrate in opposite directions within the same plane [49]. Both graphite and FLG show a prominent G-band, indicating the presence of a graphitic structure. Both samples have identical G-band positions, which is predicted given their sp^2 carbon network structure. The 2D-band ($\sim$2,700 cm^{-1}) is a second-order overtone of the D-band that corresponds to the stacking order of GO layers [27]. FLG has 2D peak which appears sharper and more intense than the graphite, indicating fewer GO layers. The form and intensity of the 2D band can also indicate the thickness of GO. The sharper peak in FLG might imply a well-ordered FLG structure [21]. In addition, Lorentzian peak fitting, as displayed in Error! Reference source not found., was applied to the D, G, and 2D bands of both spectra to further quantify the differences between graphite and FLG. The intensity ratio I_{2D}/I_G increased from $\sim$0.48 in graphite to $\sim$0.83 in FLG. The Raman spectrum of the synthesized FLG exhibited an I_{2D}/I_G ratio of 0.83 and a 2D peak FWHM of 76 cm^{-1}, suggesting an estimated GO stacking of 4 - 6 layers, supporting the classification of FLG [50].
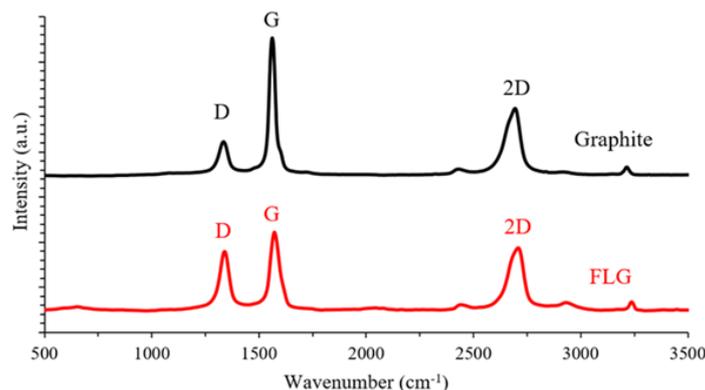
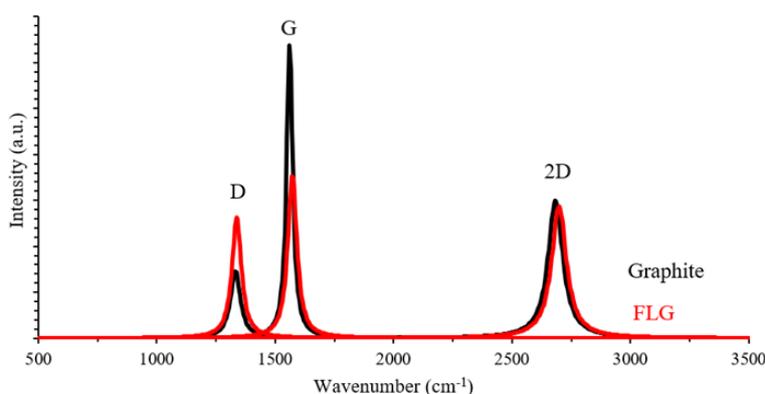**Figure 5** Comparison of Raman spectra at 532 nm for FLG and graphite.

Figure 6 Lorentzian peak fitting of Raman spectra plotted between graphite and FLG.

Error! Reference source not found. allows an XRD pattern comparison between graphite and FLG. This XRD pattern presented successful exfoliation of graphite, which is reflected in the decreased FLG peak intensity when compared to graphite. A high degree of crystallinity and ordered stacking of graphite layers are indicated by the sharp and intense peak at approximately 26.6°, which corresponds to the (002) plane of graphite. On the other hand, the peak of FLG (002) is notably less intense and broader than that of graphite, with ~ 9.02° of FWHM. This broadening suggests that graphite has successfully exfoliated into thinner layers by showing a decrease in crystallite size along the c-axis. Increased interlayer spacing is indicated by a shift of the (002) peak to a slightly lower 2θ value, which is frequently brought on by exfoliation, or by intercalation by stabilizing agents [51]. In addition, higher-order reflections of bulk graphite are represented by the additional smaller peaks at higher 2θ values, including 100 plane at 42.5°, 101 plane at 44.5°, 004 plane at 55° and 110 plane at 77°. The (100) diffraction peak in FLG,

appearing at 43°, corresponds to the in-plane periodicity of the hexagonal carbon lattice. Bragg's law defines a relationship between the X-ray beam's angle of incidence (θ), interatomic spacing (d), and wavelength (λ = 0.15418 nm), in the crystal lattice as Eq. (5):

$$n\lambda = 2d \sin\theta \qquad (5)$$

where the order of diffraction is given by the integer *n*.

Due to the regular stacking between the GO layers being disrupted by intercalation with water and the introduction of oxygen-containing functional groups from Pluronic F-127, the spacing was increased when compared to pristine GO (~0.34 nm) [52]. In FLG, this peak is significantly broadened with 2.25 of FWHM and reduced in intensity due to the reduction in lateral crystallite size and partial loss of long-range order. Moreover, the disappearance or deterioration of higher-order reflections in the FLG pattern, which are for 101, 004, and 110 planes, indicates that the layered structure

is broken, confirming disordered stacking and fewer layers [53].

These observations are consistent with findings from various studies on sonicated GO. For instance, Gürünlü *et al.* [54] showed a decrease in peak intensity and slight shifts in the (002) peak position, indicating successful exfoliation and the formation of FLG structures. Similarly, Zhang *et al.* [55] reported that the

pattern of the exfoliated GO sheets shows a superimposed reflection peak at 23.4°, corresponding to a larger interlayer spacing of lattice-damaged crystals of the GO sheets. This shift and peak broadening are attributed to misalignments and defects in the carbon layer stacks, confirming the successful exfoliation of graphite into the FLG.
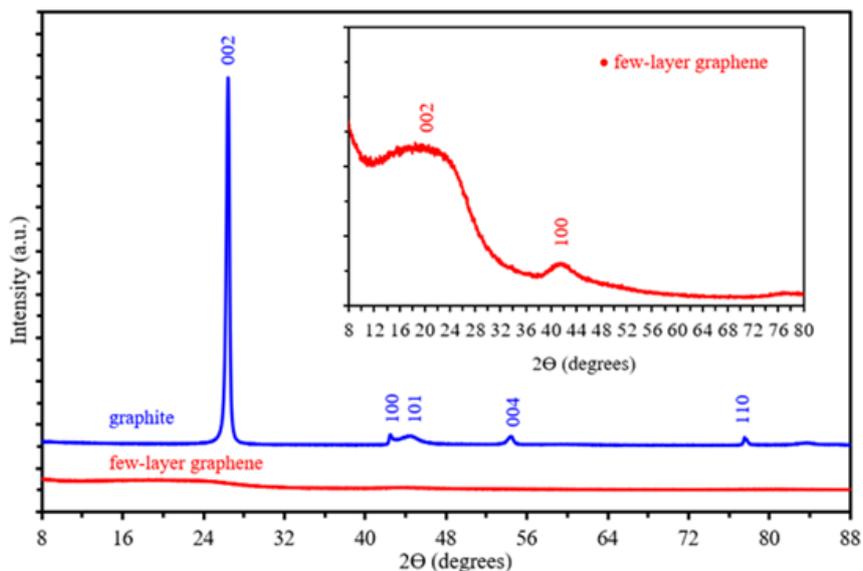

Figure 7 XRD patterns of graphite and FLG.

The electrochemical impedance spectroscopy (EIS) graph displayed in **Figure 6** highlights the performance comparison of FLG and fine graphite coating on an electrode. The Nyquist plot of FLG shows a significantly smaller semi-circular region at higher frequencies compared to fine graphite, and both have linear regions at lower frequencies, indicative of the electrode's charge transfer resistance (R_{ct}) and diffusion-controlled processes, respectively. From the inset, R_{ct} of FLG can be estimated at approximately 0.07 Ω, derived from the semicircle diameter [56]. In addition, solution resistance (R_s) of FLG and fine graphite can reach 0.45 and 2.15 Ω, respectively. The lower resistance of FLG demonstrates its higher conductivity and charge transfer efficiency.

The EIS data of FLG were fitted using the equivalent circuit shown in **Figure 6**, composed of solution resistance (R_s:R_1) corresponding to the resistance of the active substance and the electrolyte's inherent resistance, the constant phase element (CPE_1) is actually the double layer characteristic and is in

parallel with charge transfer resistance (R_{ct}:R_2), and the Warburg impedance (W_{O1}) models the diffusion of OH^- ions [57]. The parameters fit to the data are displayed in **Table 3**. The use of CPE_1 instead of an ideal capacitor reflects the non-ideal electrochemical double-layer behavior due to the surface heterogeneities of the FLG electrodes, and is defined by [58]:

$$Z_{CPE} = [Q(j\omega)^n]^{-1} \tag{6}$$

where ω is the angular frequency of the measuring signal, and Q and n are frequency-independent constants.

The constant value of Q is directly proportional to the active area and is associated with the apparent capacitance. The exponent n is a correction factor that may be connected in some way to the roughness of the electrode, with values ranging from 0 to 1, while n = 0 and 0.5 indicate resistance and Warburg behavior, respectively, with n = 1 indicating that the CPE element is an ideal capacitor. Generally, a CPE may appear as a

result of a distribution of relaxation times due to inhomogeneities at the interface between the electrode and electrolyte, porosity, and diffusion-related dynamic disorder [59]. The low R_2 of 0.07 Ω, indicates efficient ion transport and minimal interfacial resistance compared to other GO -based electrodes, where R_2

commonly is within 0.05 - 1.86 Ω [60], and the minimal Warburg component suggests efficient ion diffusion within the electrode pores. This model aligns with standard interpretations of impedance spectra in carbon-based energy storage devices [61].
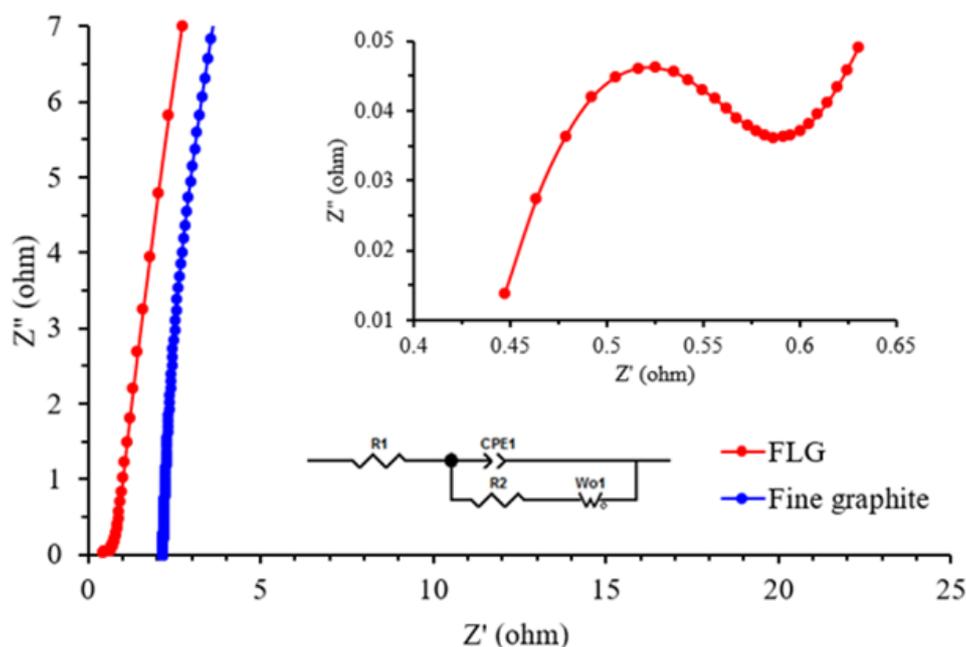

Figure 6 Equivalent circuit representation and Nyquist plot of the FLG and fine graphite coated electrode in the frequency range of 0.1 - 100,000 Hz by applying an AC at 5 mV.

Table 3 The equivalent circuit parameters identified from the impedance spectrum for FLG in **Figure 6**.

Element	Value
R_1	0.45
CPE_{1-T}	0.08
CPE_{1-P}	1.00
R_2	0.07
W_{o1-R}	0.13
W_{o1-T}	1.30
$Wo1-P$	0.41

Cyclic voltammetry (CV) analysis of symmetric supercapacitors provides important information about their charge storage behavior and electrochemical performance. CV curves with a quasi-rectangular shape at different scan rates (100 - 500 mV s^{-1}) are shown in Error! Reference source not found.. This is indicative of double-layer capacitance with negligible Faradaic contributions. Furthermore, the excellent reversibility

and stability of the electrode material are confirmed by the symmetry between the positive and negative current densities. The potential window of −1 to 1 V further reinforces the suitability of the aqueous or stable electrolyte system, as no significant Faradaic redox peaks are observed, confirming the dominance of double-layer charge storage mechanisms [62].

The galvanostatic charge-discharge (GCD) analysis is a critical method for evaluating the electrochemical performance of symmetric supercapacitors. The characteristics of the discharge curves provide insights into the charge storage mechanisms, energy efficiency, and material performance under varying current densities [62,63]. This study used GCD measurements to examine the behavior of a symmetric supercapacitor within the potential window 0 - 0.7 V, assessing its linearity, current dependence, and specific capacitance across different current densities. The discharge profiles in the GCD curves are almost linear, which is indicative of ideal capacitive behavior. The stability of the electrode material during operation and the reversibility of the system are further supported by the symmetric shape of the charge and discharge cycles [64].
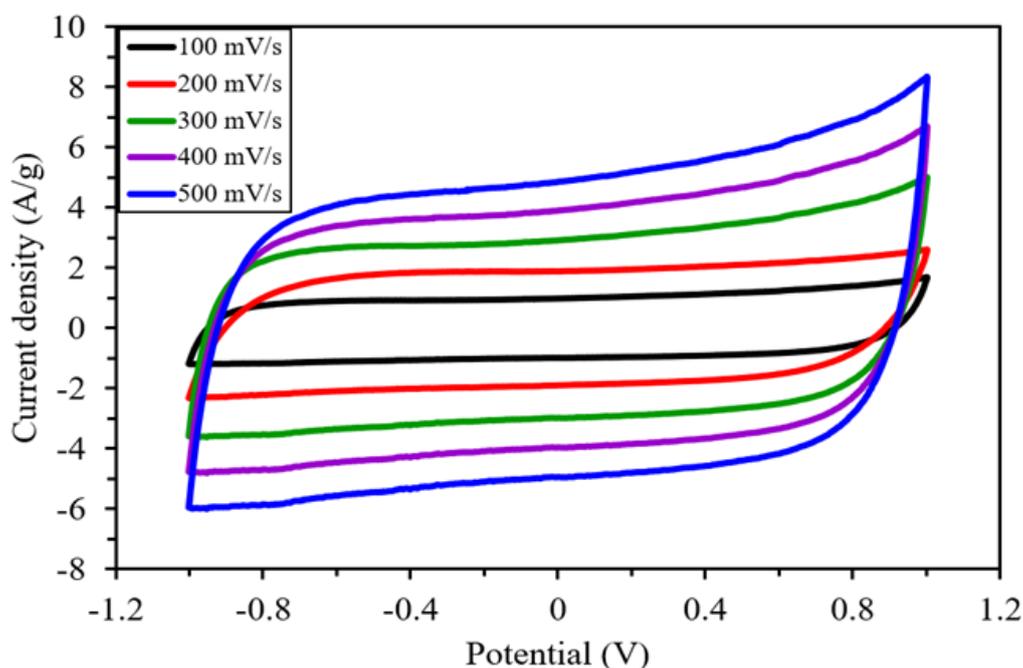

Figure 7 CV curves for FLG electrode under scan rates of 100 - 500 mV s^{-1} across the potential window from -1 to 1 V.

Error! Reference source not found. indicates that when the applied current density rises from 0.1 to 0.5 A g^{-1}, the discharge time falls considerably. Specific capacitance (C_s) is a key parameter for quantifying the charge storage capability of a supercapacitor. It can be calculated using the equation:

$$C_s = \frac{I \cdot \Delta t}{m \cdot \Delta V} \qquad (7)$$

$$Wh = \frac{1}{7200} C_s \, \Delta V^2 \qquad (8)$$

where watt-hours (Wh) are the stored energy. I represents the applied current (A), m represents the mass of active material (g), ΔV represents the potential window (V), and Δt represents the discharge time of 1 cycle (s).

Based on the discharge times extracted from the GCD curves, the findings clearly show that specific capacitance and current density are negatively correlated. At 0.1 A g^{-1}, the electrode demonstrates the highest capacitance of 71.34 F g^{-1} (4.855 mWh), reflecting efficient ion diffusion and full utilization of the active surface. However, as the current density increases to 0.2, 0.3, 0.4, and 0.5 A g^{-1}, the specific capacitance significantly decreases to 70.62, 23.44, 12.74, and 14.29 F g^{-1}, respectively. This reduction is attributed to insufficient time for the electrolyte ions to access the full surface area of the electrode at higher current rates, leading to diminished charge storage performance.

The highest specific capacitance obtained in this study, 71.34 F g^{-1} at a lower current density (0.1 A g^{-1}) with IR drop of 0.03 V, is significantly higher than the

value reported by Vika *et al.* [65] for thermally reduced graphene oxide (rGO), which exhibited 6.53 mF g^{-1} in 1M H$_2$SO$_4$ [65]. The lower capacitance of rGO may be attributed to its reduced surface area and the presence of oxygen functional groups that limit efficient charge storage. However, the capacitance of FLG in this study is lower than the 142.3 F g^{-1} achieved by Williams *et al.* [66] who used FLG as a conductive additive in activated carbon electrodes with 6 M KOH as the electrolyte. The superior performance of FLG in their study may be due to enhanced ion diffusion and charge transfer within the highly porous structure, or affected by particle size. Additionally, that study demonstrated that the high-performance supercapacitor may use alternative electrolytes with different molecular weights, such as H$_2$SO$_4$ or Na$_2$SO$_4$.
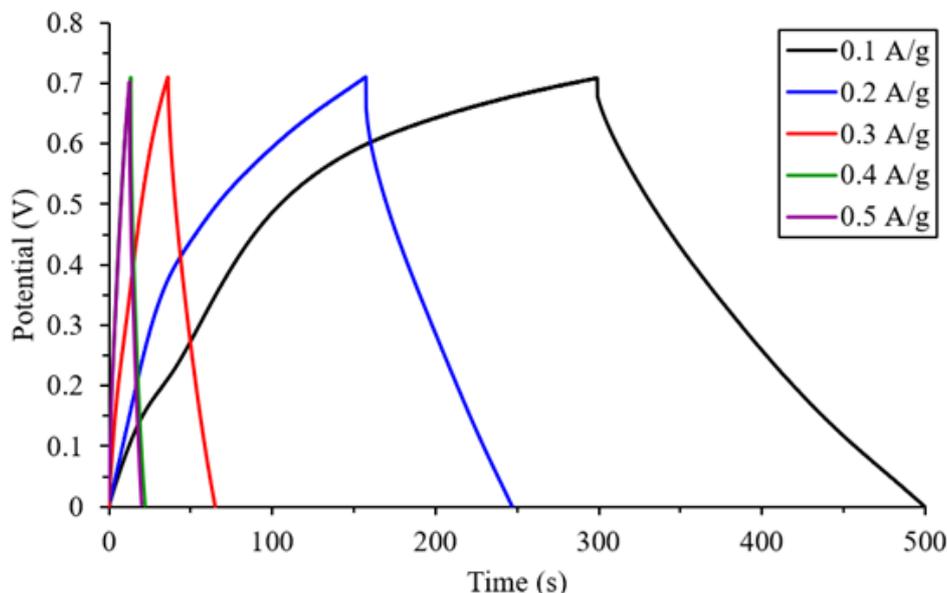

Figure 10 Charge/discharge curves for FLG electrode under various current densities within 0.1 - 0.5 A g^{-1}.

Conclusions

This study demonstrated a scalable, cost-effective method for producing FLG using mechanical exfoliation in a kitchen blender. The nanoflakes formed had approximately 400 nm diameter. The results revealed that the synthesized FLG retains high structural integrity, evidenced by Raman, FTIR, and XRD analyses. Electrochemical performance evaluations confirm the materials suitability for supercapacitor applications, with a low charge transfer resistance and excellent specific capacitance. The specific capacitance determined in this investigation was 71.34 F g^{-1} (4.855 mWh) at a low current density (0.1 Ag^{-1}) when using 6M KOH electrolyte. The synthesis process ensures minimal environmental impact and high resource efficiency, aligning with green chemistry principles. Actually, the GO is highly costly because of the complexity of the conventional processes, but the novel alternative involves simple production and formation in nano-size, ensuring comparatively low cost. These findings underline the potential for FLG as a competitive material in energy storage applications, paving the way for further industrial-scale exploration.

Acknowledgements

Declaration of Generative AI in Scientific Writing

The authors acknowledge the use of generative AI tools (ChatGPT by License AI) in the preparation of this manuscript, specifically for language editing and grammar correction. No content generation or data interpretation was performed by AI. The authors take

full responsibility for the content and conclusions of this investigation.

CRediT Author Statement

Pakhawat Insuwan: Methodology, Resources, Validation, Investigation and Writing – original draft. **Montri Luengchavanon**: Conceptualization, Methodology, Supervision, Validation, Funding acquisition, Project administration, and Writing – original draft. **Natthaporn Kaewchoothoong**: Data curation, Formal analysis, Validation, and Visualization.

References

[1] P Simon and Y Gogotsi. Materials for electrochemical capacitors. *Nature Materials* 2008; **7(11)**, 845-854.

[2] Y Zhu, S Murali, W Cai, X Li, JW Suk, JR Potts and RS Ruoff. Graphene and graphene oxide: Synthesis, properties, and applications. *Advanced Materials* 2010; **22(35)**, 3906-3924.

[3] K Ullah, BM Khan, AU Rashid and WC Oh. *Graphene based nanocomposites for supercapacitor electrodes. In*: ZM Stevic (Ed.). Updates on supercapacitors. IntechOpen, London, 2022.

[4] A Yasmin, JJ Luo and IM Daniel. Processing of expanded graphite reinforced polymer nanocomposites. *Composites Science and Technology* 2006; **66(9)**, 1182-1189.

[5] S Eigler, M Enzelberger-Heim, S Grimm, P Hofmann, W Kroener, A Geworski, C Dotzer, M Röckert, J Xiao, C Papp, O Lytken, HP Steinrück, P Müller and A Hirsch. Wet chemical synthesis of graphene. *Advanced Materials* 2013; **25(26)**, 3583-3587.

[6] TC Achee, W Sun, JT Hope, SG Quitzau, CB Sweeney, SA Shah, T Habib and MJ Green. High-yield scalable graphene nanosheet production from compressed graphite using electrochemical exfoliation. *Scientific Reports* 2018; **8(1)**, 14525.

[7] P Song, Z Cao, Y Cai, L Zhao, Z Fang and S Fu. Fabrication of exfoliated graphene-based polypropylene nanocomposites with enhanced mechanical and thermal properties. *Polymer* 2011; **52(18)**, 4001-4010.

[8] ATH Mtibe, M Mokhothu, MJ John, TC Mokhena and MJ Mochane. *Fabrication and characterization of various engineered nanomaterials. In*: CM Hussain (Ed.). Handbook of nanomaterials for industrial applications. Elsevier, Amsterdam, Switzerland, 2018, p. 151-171.

[9] CS Lee, SJ Shim and TH Kim. Scalable Preparation of Low-Defect Graphene by Urea-Assisted Liquid-Phase Shear Exfoliation of Graphte and Its Application in Doxorubicin Analysis. *Nanomaterials* 2020; **10(2)**, 267.

[10] SM Alhassan, S Qutubuddin and DA Schiraldi. Graphene arrested in laponite-water colloidal glass. *Langmuir* 2012; **28(8)**, 4009-4015.

[11] M Yi and Z Shen. Kitchen blender for producing high-quality few-layer graphene. *Carbon* 2014; **78**, 622-626.

[12] E Varrla, KR Paton, C Backes, A Harvey, RJ Smith, J McCauley and JN Coleman. Turbulence-assisted shear exfoliation of graphene using household detergent and a kitchen blender. *Nanoscale* 2014; **6(20)**, 11810-11819.

[13] DT Pérez-Álvarez, J Brown and J Stafford. Modification of kitchen blenders into controllable laboratory mixers for mechanochemical synthesis of atomically thin materials. *HardwareX* 2023; **16**, e00471.

[14] Z Ereš and S Hrabar. Low-cost synthesis of high-quality graphene in do-it-yourself cvd reactor. *Automatika* 2018; **59(3-4)**, 254-260.

[15] M Luengchavanon, L Chuenchom, W Limbut, K Kantakapun, R Choowang, C Putson, and S Chowdhury. Effect of Applied Graphene Nanosheets (Electrode) from the Electrolysis Process and Nanofiber-Based Separator (Electrolyte) from an Electrospinning Technique for High-Performance Supercapacitor. *ACS Omega* 2025; **10(29)**, 31348−31358.

[16] M Lotya, PJ King, U Khan, S De and JN Coleman. High-concentration, surfactant-stabilized graphene dispersions. *ACS Nano* 2010, **4(6)**, 3155-3162.

[17] L Guardia, MJ Fernández-Merino, JI Paredes, P Solís-Fernández, S Villar-Rodil, A Martínez-Alonso and JMD Tascón. High-throughput production of pristine graphene in an aqueous

dispersion assisted by non-ionic surfactants. *Carbon* 2011; **49(5)**, 1653-1662.

[18] KR Paton, E Varrla, C Backes, RJ Smith, U Khan, A O'Neill, C Boland, M Lotya, OM Istrate, P King, T Higgins, S Barwich, P May, P Puczkarski, I Ahmed, M Moebius, H Pettersson, E Long, J Coelho, SE O Brien, EK McGuire, BM Sanchez, GS Duesberg, N McEvoy, TJ Pennycook, C Downing, A Crossley, V Nicolosi and JN Coleman. Scalable production of large quantities of defect-free few-layer graphene by shear exfoliation in liquids. *Nature Materials* 2014; **13(6)**, 624-630.

[19] PG Karagiannidis, SA Hodge, L Lombardi, F Tomarchio, N Decorde, S Milana, I Goykhman, Y Su, S Mesite, D Johnstone, RK Leary, PA Midgley, NM Pugno, F Torrisi and AC Ferrari. Microfluidization of graphite and formulation of graphene-based conductive inks. *ACS Nano* 2016; **11(3)**, 2742-2755

[20] U Khan, H Porwal, A O'Neill, K Nawaz, P May and JN Coleman. Solvent-exfoliated graphene at extremely high concentration. *Langmuir* 2011; **27(15)**, 9077-9082.

[21] AC Ferrari, JC Meyer, V Scardaci, C Casiraghi, M Lazzeri, F Mauri, S Piscanec, D Jiang, KS Novoselov, S Roth and AK Geim. Raman spectrum of graphene and graphene layers. *Physical Review Letters* 2006; **97(18)**, 187401.

[22] A Mendhe and HS Panda. A review on electrolytes for supercapacitor device. *Discover Materials* 2023; **3(1)**, 29.

[23] R Kötz and M Carlen. Principles and applications of electrochemical capacitors. *Electrochimica Acta* 2000; **45(15-16)**, 2483-2498.

[24] RJ Smith, M Lotya and JN Coleman. The importance of repulsive potential barriers for the dispersion of graphene using surfactants. *New Journal of Physics* 2010; **12**, 125008.

[25] C Backes, KR Paton, D Hanlon, S Yuan, MI Katsnelson, J Houston, RJ Smith, D McCloskey, JF Donegan and JN Coleman. Spectroscopic metrics allow *in situ* measurement of mean size and thickness of liquid-exfoliated few-layer graphene nanosheets. *Nanoscale* 2016; **8(7)**, 4311-4323.

[26] U Khan, A O'Neill, M Lotya, S De and JN Coleman. High-concentration solvent exfoliation of graphene. *Small* 2010; **6(7)**, 864-871.

[27] J Phiri, P Gane and TC Maloney. High-concentration shear-exfoliated colloidal dispersion of surfactant-polymer-stabilized few-layer graphene sheets. *Journal of Materials Science* 2017; **52(13)**, 8321-8337.

[28] L Liu, Z Shen, M Yi, X Zhang and S Ma. A green, rapid and size-controlled production of high-quality graphene sheets by hydrodynamic forces. *RSC Advances* 2014; **4(69)**, 36464-36470.

[29] W Zhang, W He and X Jing. Preparation of a stable graphene dispersion with high concentration by ultrasound. *The Journal of Physical Chemistry B* 2010; **114(32)**, 10368-10373.

[30] W Liu, VA Tanna, BM Yavitt, C Dimitrakopoulos and HH Winter. Fast production of high-quality graphene via sequential liquid exfoliation. *ACS Applied Materials & Interfaces* 2015; **7(49)**, 27027-27030.

[31] M Döbbelin, A Ciesielski, S Haar, S Osella, M Bruna, A Minoia, L Grisanti, T Mosciatti, F Richard, EA Prasetyanto, LD Cola, V Palermo, R Mazzaro, V Morandi, R Lazzaroni, AC Ferrari, D Beljonne and P Samorì. Light-enhanced liquid-phase exfoliation and current photoswitching in graphene-azobenzene composites. *Nature Communications* 2016; **7(1)**, 11090.

[32] H Ma, Z Shen, M Yi, S Ben, S Liang, L Liu, Y Zhang, X Zhang and S Ma. Direct exfoliation of graphite in water with addition of ammonia solution. *Journal of Colloid and Interface Science* 2017; **503**, 68-75.

[33] J Tian, L Guo, X Yin and W Wu. The liquid-phase preparation of graphene by shear exfoliation with graphite oxide as a dispersant. *Materials Chemistry and Physics* 2019; **223**, 1-8.

[34] CS Lee, SJ Shim and TH Kim. Scalable preparation of low-defect graphene by urea-assisted liquid-phase shear exfoliation of graphite and its application in doxorubicin analysis. *Nanomaterials* 2020; **10(2)**, 267.

[35] JN Israelachvili. *Intermolecular and surface forces*. Academic Press, Cambridge, 2011, p. 506-550.

[36] PD Gennes. Polymers at an interface; a simplified view. *Advances in Colloid and Interface Science* 1987; **27(3-4)**, 189-209.

[37] S Wang, M Yi and Z Shen. The effect of surfactants and their concentration on the liquid exfoliation of graphene. *RSC Advances* 2016; **6(61)**, 56705-56710.

[38] M Yi, Z Shen and J Zhu. A fluid dynamics route for producing graphene and its analogues. *Chinese Science Bulletin* 2014; **59(16)**, 1794-1799.

[39] TS Tran, SJ Park, SS Yoo, TR Lee and TY Kim. High shear-induced exfoliation of graphite into high quality graphene by taylor-couette flow. *RSC Advances* 2016; **6(15)**, 12003-12008.

[40] M Ma, L Cheng, A Zhao, H Zhang and A Zhang. Pluronic-based graphene oxide-methylene blue nanocomposite for photodynamic/photothermal combined therapy of cancer cells. *Photodiagnosis and Photodynamic Therapy* 2020; **29**, 101640.

[41] KS Novoselov, AK Geim, SV Morozov, D Jiang, Y Zhang, SV Dubonos, IV Grigorieva and AA Firsov. Electric field effect in atomically thin carbon films. *Science* 2004; **306(5696)**, 666-669.

[42] JA Garlow, LK Barrett, L Wu, K Kisslinger, Y Zhu and JF Pulecio. Large-area growth of turbostratic graphene on Ni(111) via physical vapor deposition. *Scientific Reports* 2016; **6(1)**, 19804.

[43] U Khan, A O'Neill, H Porwal, P May, K Nawaz and JN Coleman. Size selection of dispersed, exfoliated graphene flakes by controlled centrifugation. *Carbon* 2012; **50(2)**, 470-475.

[44] LM Malard, MA Pimenta, G Dresselhaus and MS Dresselhaus. Raman spectroscopy in graphene. *Physics Reports* 2009; **473(5)**, 51-87.

[45] T Shimada, T Sugai, C Fantini, M Souza, LG Cançado, A Jorio, MA Pimenta, R Saito, A Grüneis, G Dresselhaus, M. Dresselhaus, Y Ohno, T Mizutani and H Shinohara. Origin of the 2450 cm^{-1} raman bands in hopg, single-wall and double-wall carbon nanotubes. *Carbon* 2005; **43**, 1049-1054.

[46] DL Mafra, G Samsonidze, LM Malard, DC Elias, JC Brant, F Plentz, ES Alves and MA Pimenta. Determination of la and to phonon dispersion relations of graphene near the dirac point by double resonance raman scattering. *Physical Review B* 2007; **76(23)**, 233407.

[47] AA Green and MC Hersam. Solution phase production of graphene with controlled thickness via density differentiation. *Nano Letters* 2009; **9(12)**, 4031-4036.

[48] SE Veras, E Espada, S Collazo, M Grau, R Katiyar, VI Makarov, BR Weiner and G Morell. Hydrogenated graphene systems: A novel growth and hydrogenation process. *Carbon Trends* 2024; **15**, 100360.

[49] K Ishimaru, T Hata, P Bronsveld, T Nishizawa and Y Imamura. Characterization of sp2- and sp3-bonded carbon in wood charcoal. *Journal of Wood Science* 2007; **53(5)**, 442-448

[50] Y Liu, Z Liu, WS Lew and QJ Wang. Temperature dependence of the electrical transport properties in few-layer graphene interconnects. *Nanoscale Research Letters* 2013; **8(1)**, 335.

[51] JLS Gascho, SF Costa, AAC Recco and SH Pezzin. Graphene oxide films obtained by vacuum filtration: X-ray diffraction evidence of crystalline reorganization. *Journal of Nanomaterials* 2019; **2019(1)**, 5963148.

[52] HH Huang, KKHD Silva, GRA Kumara and M Yoshimura. Structural evolution of hydrothermally derived reduced graphene oxide. *Scientific Reports* 2018; **8(1)**, 6849.

[53] RM Allaf, IV Rivero, SS Spearman and LJ Hope-Weeks. On the preparation of as-produced and purified single-walled carbon nanotube samples for standardized x-ray diffraction characterization. *Materials Characterization* 2011; **62(9)**, 857-864.

[54] B Gürünlü, Ç Taşdelen-Yücedağ and M Bayramoğlu. Graphene synthesis by ultrasound energy-assisted exfoliation of graphite in various solvents. *Crystals* 2020; **10(11)**, 1037.

[55] R Zhang, B Zhang and S Sun. Preparation of high-quality graphene with a large-size by sonication-free liquid-phase exfoliation of graphite with a new mechanism. *RSC Advances* 2015; **5(44)**, 783-791.

[56] R Weber, AJ Louli, KP Plucknett and JR Dahn. Resistance growth in lithium-ion pouch cells with LiNi$_{0.80}$Co$_{0.15}$Al $_{0.05}$O$_2$ positive electrodes and proposed mechanism for voltage dependent

charge-transfer resistance. *Journal of the Electrochemical Society* 2019; **166**, A1779.

[57] M Faraji and F Gobal. Preparation and electrochemical performances of nanoporous/cracked cobalt oxide layer for supercapacitors. *Applied Physics A* 2014; **117(4)**, 2087-2094.

[58] C Xia, Y Xie, Y Wang, W Wang, H Du and F Tian. Preparation and capacitance performance of polyaniline/titanium nitride nanotube hybrid. *Journal of Applied Electrochemistry* 2013; **43**, 1225-1233.

[59] T Girija and M Sangaranarayanan. Analysis of polyaniline-based nickel electrodes for electrochemical supercapacitors. *Journal of Power Sources* 2006; **156(2)**, 705-711.

[60] S Breitenbach, A Lumetzberger, MA Hobisch, C Unterweger, S Spirk, D Stifter, C Fürst and AW Hassel. Supercapacitor electrodes from viscose-based activated carbon fibers: Significant yield and performance improvement using diammonium hydrogen phosphate as impregnating agent. *C* 2020; **6(2)**, 17.

[61] Y Barsukov and J Macdonald. Impedance spectroscopy: Theory, experiment, and applications. *Journal of the American Chemical Society* 2005; **127(35)**, 12431.

[62] MMM Mohammed and DM Chun. Electrochemical performance of few-layer graphene nano-flake supercapacitors prepared by the vacuum kinetic spray method. *Coatings* 2018; **8(9)**, 302.

[63] MAAM ABID, MI Radzi, M Mupit, H Osman, RF Munawar, KF Samat, MSM Suan, K Isomura and M Islam. Cyclic voltammetry and galvanostatic charge-discharge analyses of polyaniline/graphene oxide nanocomposite based supercapacitor. *Malaysian Journal on Composites Science and Manufacturing* 2020; **3(1)**, 14-26.

[64] S Teng, G Siegel, W Wang and A Tiwari. Carbonized wood for supercapacitor electrodes. *ECS Solid State Letters* 2014; **3(5)**, M25-M28.

[65] V Marcelina, N Syakir, S Wyantuti, YW Hartati and R Hidayat. Characteristic of thermally reduced graphene oxide as supercapacitors electrode materials. *IOP Conference Series: Materials Science and Engineering* 2017; **196(1)**, 012034.

[66] RE Williams, S Sukumaran, Q Abbas and MRC Hunt. Few-layer graphene as an 'active' conductive additive for flexible aqueous supercapacitor electrodes. *Carbon* 2024; **218**, 118744.